CellPress
PARTNER JOURNAL

Molecular Plant
Research Article

Interactions between Transmembrane Helices within Monomers of the Aquaporin AtPIP2;1 Play a Crucial Role in Tetramer Formation

Yun-Joo Yoo[1], Hyun Kyung Lee[2], Wonhee Han[2], Dae Heon Kim[3], Myoung Hui Lee[4], Jouhyun Jeon[2], Dong Wook Lee[4], Junho Lee[2], Yongjik Lee[4], Juhun Lee[4], Jin Seok Kim[2], Yunje Cho[2], Jin-Kwan Han[2] and Inhwan Hwang[1,2,4,*]

[1]School of Interdisciplinary Bioscience and Bioengineering, Pohang University of Science and Technology, Pohang 790-784, Korea

[2]Department of Life Sciences, Pohang University of Science and Technology, Pohang 790-784, Korea

[3]Department of Biology, Sunchon National University, Sunchon 57922, Korea

[4]Division of Integrative Biosciences and Biotechnology, Pohang University of Science and Technology, Pohang 790-784, Korea

***Correspondence: Inhwan Hwang (ihhwang@postech.ac.kr)**

http://dx.doi.org/10.1016/j.molp.2016.04.012

ABSTRACT

Aquaporin (AQP) is a water channel protein found in various subcellular membranes of both prokaryotic and eukaryotic cells. The physiological functions of AQPs have been elucidated in many organisms. However, understanding their biogenesis remains elusive, particularly regarding how they assemble into tetramers. Here, we investigated the amino acid residues involved in the tetramer formation of the *Arabidopsis* plasma membrane AQP AtPIP2;1 using extensive amino acid substitution mutagenesis. The mutant proteins V41A/E44A, F51A/L52A, F87A/I91A, F92A/I93A, V95A/Y96A, and H216A/L217A, harboring alanine substitutions in the transmembrane (TM) helices of AtPIP2;1 polymerized into multiple oligomeric complexes with a variable number of subunits greater than four. Moreover, these mutant proteins failed to traffic to the plasma membrane, instead of accumulating in the endoplasmic reticulum (ER). Structure-based modeling revealed that these residues are largely involved in interactions between TM helices within monomers. These results suggest that inter-TM interactions occurring both within and between monomers play crucial roles in tetramer formation in the AtPIP2;1 complex. Moreover, the assembly of AtPIP2;1 tetramers is critical for their trafficking from the ER to the plasma membrane, as well as water permeability.

Key words: aquaporin, AtPIP2, tetramer formation, interaction between transmembrane helices

Yoo Y.-J., Lee H.K., Han W., Kim D.H., Lee M.H., Jeon J., Lee D.W., Lee J., Lee Y., Lee J., Kim J.S., Cho Y., Han J.-K., and Hwang I. (2016). Interactions between Transmembrane Helices within Monomers of the Aquaporin AtPIP2;1 Play a Crucial Role in Tetramer Formation. Mol. Plant. **9**, 1004–1017.

INTRODUCTION

Aquaporins (AQPs) are a family of membrane proteins that function as water channels. These proteins are highly conserved and widely distributed throughout both prokaryotes and eukaryotes, comprising large protein families with 35 members in *Arabidopsis* and 13 members in humans (Kaldenhoff and Fischer, 2006; Maurel, 2007; Maurel et al., 2008; Gomes et al., 2009). AQPs are found in various cellular membranes, such as the plasma membrane (PM), the tonoplasts, and the endoplasmic reticulum (ER) membrane, indicating that they are involved in water transport across these biological membranes (Maeshima and Ishikawa, 2008). These water transport proteins are involved in various physiological processes, such as water reabsorption during urine production in the kidney, water balance in various animal tissues, and the control of water status in plants (Zador et al., 2007; Kaldenhoff et al., 2008; Ishibashi et al., 2009). Although the majority of AQPs exhibit water-conducting activity, certain members of the AQP family such as aquaglyceroporins are involved in the transport of other small molecules such as glycerol, boron, silicon, and other small organic metabolites (Takano et al., 2006; Rojek et al., 2008; Tanaka et al., 2008; Gomes et al., 2009; Mitani et al., 2009).

The molecular mechanism underlying the water-conducting activity of AQPs has been elucidated at various levels. The atomic

Published by the Molecular Plant Shanghai Editorial Office in association with Cell Press, an imprint of Elsevier Inc., on behalf of CSPB and IPPE, SIBS, CAS.

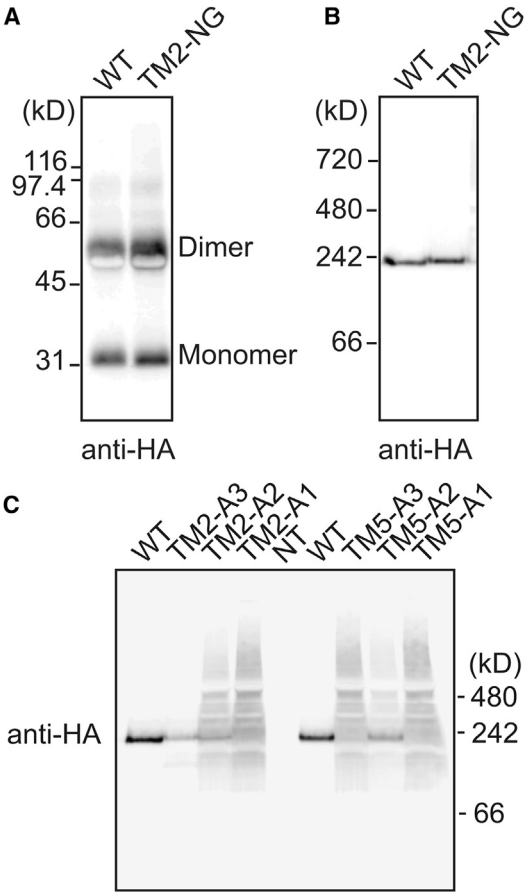

Figure 1. Glycine Substitution of the N-Terminal Flanking Region of TM2 Does Not Affect Tetramer Formation in AtPIP2;1.

(A) Expression of TM2-NG:HA in protoplasts. Protein extracts from protoplasts transformed with *TM2-NG:HA* or WT *AtPIP2;1:HA* were separated by SDS–PAGE and analyzed by western blotting using anti-HA antibody.

(B) Formation of TM2-NG:HA tetramers. Protein extracts from protoplasts transformed with *TM2-NG:HA* or WT *AtPIP2;1:HA* were separated by BN–PAGE and analyzed by western blotting using anti-HA antibody.

(C) Effect of mutations on tetramer formation. Protoplasts were transformed with the indicated constructs, and protein extracts were separated by BN–PAGE, followed by western blot analysis using anti-HA antibody. WT, AtPIP2;1:HA; TM2-A1, TM2-A1:HA; TM2-A2, TM2-A2:HA; TM2-A3, TM2-A3:HA; TM5-A1, TM5-A1:HA; TM5-A2, TM5-A2:HA; TM5-A3, TM5-A3:HA. NT, non-transformed protoplasts.

structures of various AQPs and aquaglyceroporins have provided a basis for developing a molecular model describing how water is transported through the pores of AQPs (Fu et al., 2000; Sui et al., 2001; Tajkhorshid et al., 2002; Savage et al., 2003; Hedfalk et al., 2006; Törnroth-Horsefield et al., 2006; Yu et al., 2006). These studies revealed that homo- or hetero- tetramer formation is critical for the water channel activity of these proteins, although the pore in each subunit is responsible for the passage of water and small molecules (Mathai and Agre, 1999; Duchesne et al., 2001; de Groot and Grubmuller, 2001; Duchesne et al., 2002; Tajkhorshid et al., 2002; Zelazny et al., 2007; Sorieul et al., 2011). However, the exact mechanism for the assembly of tetramers and higher oligomeric forms is not clearly understood at the molecular level (Duchesne et al., 2002; Buck et al., 2007). How AQPs are assembled into tetramers and how they exist as stable complexes are fundamental questions that remain to be answered. Multiple sequence motifs located at the loop regions play a crucial role in the stability of HsAQP1 and *Cicadella* aquaporin (AQPcic) tetramers (Duchesne et al., 2001; Buck et al., 2007). In addition, the large area of interface between AQP monomers contributes to the stability of tetramers (Törnroth-Horsefield et al., 2006). However, it is not clear whether the mechanisms employed by HsAQP1 and AQPcic to generate tetramers can also be applied to other AQPs. Although AQPs are highly conserved proteins, significant sequence divergence is present in the primary sequences of numerous AQPs, which precludes deducing sequence motifs involved in tetramer formation based on sequence homology (Gomes et al., 2009). In this study, we investigated the structural features involved in the assembly of *Arabidopsis* PM AQP AtPIP2;1 tetramers. We generated a large number of amino acid substitution mutants of AtPIP2;1 to identify sequence motifs involved in tetramer assembly. We identified many residues in TM helices that are involved in the formation of AtPIP2;1 tetramers from homomeric complexes. Subsequently, through structure modellingof AtPIP2;1, we determined that these critical residues are involved in TM helix–helix interactions within monomers as well as between monomers. Finally, we provide evidence that tetramer formation is critical for AtPIP2;1 trafficking from the ER to the PM, as well as water permeability, in *Arabidopsis*.

RESULTS

AtPIP2;1 TM Helices Play Crucial Roles in Tetramer Formation

To gain insight into the mechanism of AtPIP2;1 tetramer formation, we initially compared the amino acid sequence of AtPIP2;1 with that of human aquaporin 1 (HsAQP1), which harbors two regions that play critical roles in tetramer formation (Buck et al., 2007). One region comprises two amino acid residues, asparagine (N49) and lysine (K51), which are immediately adjacent (on the N-terminal side) to transmembrane domain 2 (TM2), while the other comprises aspartate (D185) on the C-terminal side of TM5. These amino acid residues in AQP1 are not conserved in AtPIP2;1 (Supplemental Figure 1). Nevertheless, we examined whether the N-terminal flanking region of TM2 in AtPIP2;1 contains amino acid residues involved in tetramer formation. We generated the mutant protein TM2-NG by substituting eight amino acids of the N-terminal flanking region of TM2 with glycines; the resulting construct was fused to HA at the C terminus to generate TM2-NG:HA. The construct was introduced into protoplasts from leaf tissues by polyethylene glycol-mediated transformation (Jin et al., 2001; Kim et al., 2001). Recently, this protoplast system was successfully used to examine the targeting of AtPIP2;1 and ZmPIP2s (as GFP fusion proteins) to the PM (Zelazny et al., 2007, 2009; Lee et al., 2009; Besserer et al., 2012; Bienert et al., 2012; Chevalier et al., 2014). First, we examined the expression of these constructs in protoplasts. Protein extracts from protoplasts were separated by SDS–PAGE and analyzed by western blotting using anti-HA antibody. Both wild-type (WT) and TM2-NG:HA proteins produced strong bands at 33 and 57 kDa corresponding to monomers and dimers, respectively, when analyzed by SDS–PAGE after denaturation with SDS (Figure 1A). Next, we examined tetramer formation using these protein extracts by blue native gel electrophoresis (BN–PAGE), followed by western blot analysis

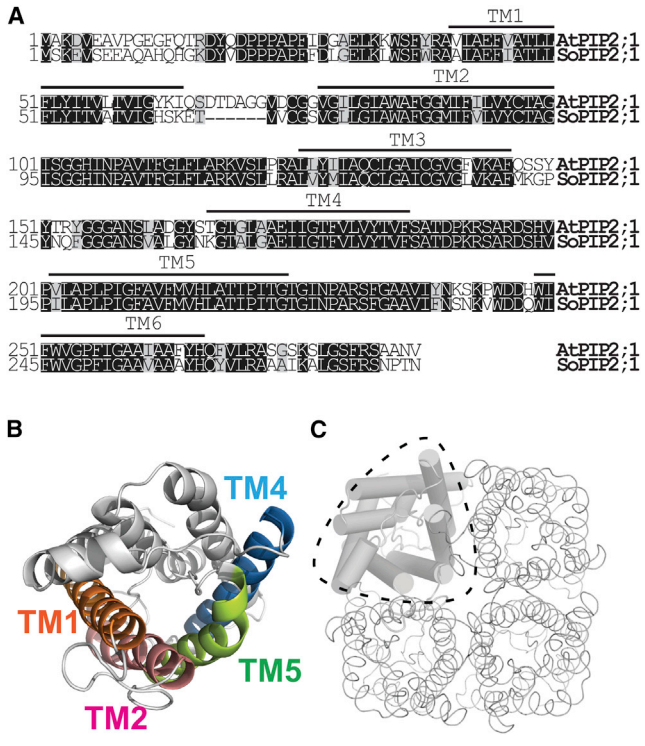

Figure 2. Generation of a Model Structure of AtPIP2;1.

(A) Sequence alignment between AtPIP2;1 and SoPIP2;1. Amino acid residues highlighted in black and gray boxes indicate identical and conserved residues, respectively, between two sequences. AtPIP2;1 shares 75.3% amino acid identity with SoPIP2;1. Black lines indicate the TM region.

(B) The structure of the AtPIP2;1 monomer. The structure of AtPIP2;1 was modeled based on that of SoPIP2;1 by homology modeling.

(C) The structure of the AtPIP2;1 tetramer. The area indicated by a dashed line contains the monomer. Four monomers are assembled into a tetramer.

using anti-HA antibodies. Previously, BN–PAGE has been used to examine the complex formation of various membrane proteins including AQPs (Kjell et al., 2004; Wittig et al., 2006). TM2-NG:HA proteins produced a band at the same position (approximately 240 kDa) as that of AtPIP2;1:HA (Figure 1B). Previous studies have shown that AQPs migrate to approximately 240 kDa in blue native gels (Kjell et al., 2004). Therefore, these results strongly suggest that the N-terminal flanking region of TM2 does not contain a sequence motif for tetramer formation.

Next, we focused on the hydrophobic TM helices of AtPIP2;1. Structural analysis suggested that in addition to their role in membrane insertion, the TM helices of AQPs, particularly TM2 and TM5, play a crucial role in subunit interactions (Törnroth-Horsefield et al., 2006). Thus, we examined the importance of TMs in tetramer assembly. To roughly deduce their role in tetramer assembly, we initially substituted nine to ten amino acid residues in TM2 or TM5 with the corresponding number of alanines (TM2-A1:HA to TM2-A3:HA mutants of TM2, and TM5-A1:HA to TM5-A3:HA mutants of TM5) (Supplemental Figure 2). In previous studies, multiple alanine substitutions in the TMs of single TM-containing membrane proteins did not affect their insertion into membranes (Lee et al., 2001; Hessa et al., 2009). We analyzed these mutant proteins by BN–PAGE. All alanine substitution mutants, except for TM2-A3, produced banding patterns that were different from those of WT proteins (Figure 1C); the mutants produced multiple, discrete bands above the tetramers together with a smeared band at the top of the gel. This result suggests that TM2 and TM5 contain residues that are crucial for tetramer formation of subunits in the AtPIP2;1 complexes. However, we cannot rule out the possibility that the substitution of large numbers of TM residues with alanine may cause a gross distortion in the structure of TM helices, thereby resulting in non-specific protein aggregates and abnormal migration patterns in the gel. Thus, we investigated whether these proteins are properly inserted into membranes by examining protein topology. We chose TM2-A2 as a representative mutant protein with abnormal gel migration patterns. We examined the topology of this mutant by tagging it with GFP at its C terminus and transforming the resulting construct, *TM2-A2:GFP*, into protoplasts. We then subjected the protein extracts from transformed protoplasts to thermolysin treatment. GFP-tagged WT AtPIP2;1 (AtPIP2;1:GFP) and ST:GFP, a marker of the Golgi apparatus (Kim et al., 2001), were used as controls and had their GFP moiety exposed to the cytosol and lumen, respectively. For both WT and mutant AtPIP2;1:GFP proteins, the C-terminal GFP moiety was released from the AtPIP2;1 proteins to a similar extent upon thermolysin treatment (Supplemental Figure 3), indicating that the GFP moiety was exposed to the cytosol. The negative control, ST:GFP, was resistant to protease treatment. These results suggest that TM2-A2 seems to be properly inserted into the membranes as WT AtPIP2;1, thus ruling out the possibility that the abnormal gel migration pattern of these mutants was caused by non-specific protein aggregation.

TM1, TM2, and TM5 Contain Amino Acid Residues Involved in Tetramer Formation of AtPIP2;1

The results shown in Figure 1 prompted us to search for the sequence motifs in the TM domains those are involved in tetramer formation more systematically. Previous structural analysis of AQP revealed that the TM helices of various AQPs interact within and between monomers (Törnroth-Horsefield et al., 2006). We hypothesized that the interaction between TM helices is an important structural feature for tetrameric assembly of AtPIP2;1. First, we generated a model structure of AtPIP2;1, since no structural information for AtPIP2;1 was available. Spinach PIP2;1 (SoPIP2;1) is the only plant aquaporin whose structure has been determined to date (Törnroth-Horsefield et al., 2006; Nyblom et al., 2009). Since the primary amino acid sequence of AtPIP2;1 is highly similar to that of SoPIP2;1 (Figure 2A), we generated a model structure of AtPIP2;1 based on SoPIP2;1 (PDB: 3CN6) using Swiss Model (Figure 2B). We then focused on residues predicted to be involved in interactions between neighboring TM helices using the AtPIP2;1 model structure. If residues in two neighboring TM helices were located within 5 Å, they were considered to have a van der Waals interaction (Supplemental Table 2). As shown in Supplemental Table 2, most residues of TM1, TM2, TM4, and TM5 can interact with other TMs.

To investigate whether these predicted inter-TM interactions are important for the formation of AtPIP2;1 tetramers, we substituted the TM residues predicted to have inter-TM interactions with

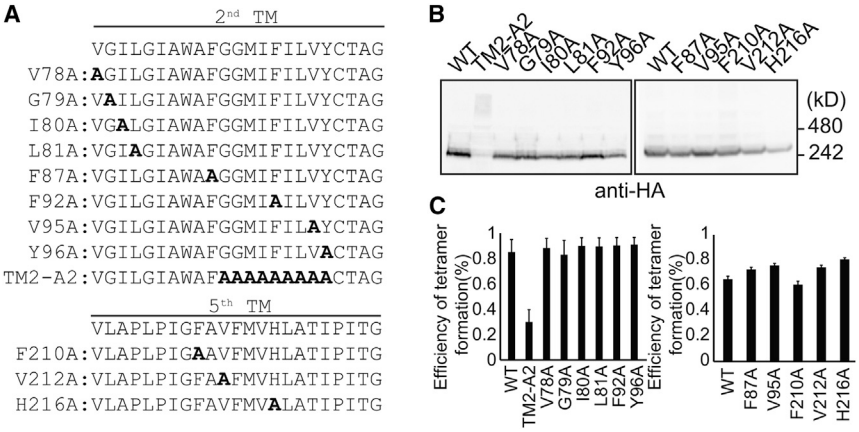

Figure 3. Single Alanine Substitution Mutations in TM2 and TM5 Do Not Affect AtPIP2;1 Tetramer Formation.

(A) Amino acid sequences of single alanine substitution mutants. The amino acid residues substituted with alanine are as indicated. TM2-A2, AtPIP2;1[TM2-A2]:HA. Bold letters indicate alanine substitution.

(B) Effect of single substitution mutants on tetramer formation. Protoplasts were transformed with the indicated constructs, and protein extracts were separated by blue native gel electrophoresis, followed by western blot analysis using an anti-HA antibody. WT, AtPIP2;1:HA.

(C) Quantification of tetramer formation efficiency. To quantify the efficiency of tetramer formation, the tetramer band intensity was measured using LAS3000 software. The efficiency of tetramer assembly is expressed as the relative value over total expressed proteins. The values are means with SE (n = 2).

alanines. First, we generated eight single alanine substitution mutants (V78A, G79A, I80A, L81A, F87A, F92A, V95A, and Y96A) of TM2 and three single mutants (F210A, V212A, and H216A) of TM5 (Figure 3A). The 11 residues selected for alanine substitution were predicted to have one-to-six inter-TM interactions (Supplemental Table 2). The resulting mutant constructs were tagged with HA at the C terminus and expressed in protoplasts. We analyzed protein extracts from these protoplasts by western blot using anti-HA antibody (Figure 3B), finding that the mutant proteins were expressed at WT levels. Next, we examined tetramer formation of these mutants by BN–PAGE, followed by western blot analysis using anti-HA antibody (Figure 3B). All the single alanine substitution mutants produced tetramers at more than 80% efficiency, which is comparable with that of WT AtPIP2;1 (Figure 3C). Perhaps the residues substituted with alanine are not crucial for tetramer assembly. Alternatively, alanine substitution of single residues in TM2 and TM5 helices may be tolerable for tetramer assembly.

To identify the residues involved in tetramer assembly, we generated double and triple substitution mutants by replacing two or three residues that were predicted to be partners in inter-TM interactions (I83A/I220A, W85A/F210A, V95A/I208A, V95A/V202A/I203A) (Figure 4A and 4B). The resulting mutant constructs were tagged with HA at the C terminus and expressed in protoplasts. We analyzed protein extracts from these protoplasts by western blot using anti-HA antibody (Figure 4C), finding that all mutant proteins were readily expressed at WT levels in protoplasts (Supplemental Figure 4). Next, we examined tetramer formation using these mutants by BN–PAGE (Figure 4C). The mutants produced tetramers at levels similar to, or only slightly lower than, that of WT AtPIP2;1 (Figure 4D), indicating that the absence of a single interaction between TMs does not affect tetramer assembly.

As an alternative approach, we introduced double substitution mutations by replacing a pair of the two nearest residues in the same TM helix, each of which has at least two interactions with residues in a neighboring TM helix, sequentially throughout the TM. We examined tetramer formation in eight TM1 mutants, including V41A/E44A:HA, F45A/T48A:HA, L49A/L50A:HA, F51A/L52A:HA, Y53A/I54A:HA, T55A/V56A:HA, L57A/T58A:HA, and V59A/Y62A:HA (Figure 5A). First, we examined the expression of these constructs in protoplasts by western blot analysis using anti-HA antibody (Figure 5B). All mutant constructs except *Y53A/I54A:HA* were expressed at levels similar to WT *AtPIP2;1:HA*, whereas *Y53A/I54A:HA* was expressed at almost undetectable levels (Supplemental Figure 4). Next, we separated all the double alanine substitution mutants (except Y53A/I54A:HA) by BN–PAGE, followed by western blot using anti-HA antibody. Of the seven mutants, F45A/T48A:HA, L49A/L50A:HA, T55A/V56A:HA, L57A/T58A:HA, and V59A/Y62A:HA produced tetramers at more than 60% efficiency, which is similar to that of WT AtPIP2;1:HA. However, two mutants, V41A/E44A:HA and F51A/L52A:HA, produced tetramers at less than 20% efficiency, which is strikingly different from the assembly of WT protein but similar to that of the mutant TM2-A2:HA (Figure 5B). These two mutants produced multiple discrete and smeared bands above the tetramers, indicating that these mutants assembled into multiple oligomeric forms of the AtPIP2;1 complex.

We examined the nature of the multiple discrete and smeared bands above the tetramer. One possibility is that they represented simple aggregates of AtPIP2;1:HA mutants caused by the mutations. The second possibility is that they were specific complexes with higher, but not defined, numbers of subunits. To distinguish between these possibilities, we analyzed the mutant V41A/E44A:HA by two-dimensional gel electrophoresis, i.e., BN–PAGE in the first dimension, followed by SDS–PAGE in the second dimension (Figure 5D). WT protein was included as a control. WT protein produced two bands of nearly equal intensity at positions 33 kDa and 57 kDa, corresponding to the monomer and dimer, respectively. Dimer bands are produced by a disulfide bond between subunits of tetramers (Bienert et al., 2012). In the case of V41A/E44A:HA, all the multiple discrete and smeared bands above the tetramer observed in the blue native gel also produced monomers and dimers. However, unlike WT proteins, for V41A/E44A:HA, the monomer band was more intense than the dimer band (Figure 5C), indicating that the high molecular weight complexes above the tetramer were more easily resolved into monomers than tetramers in the second SDS–PAGE compared with WT

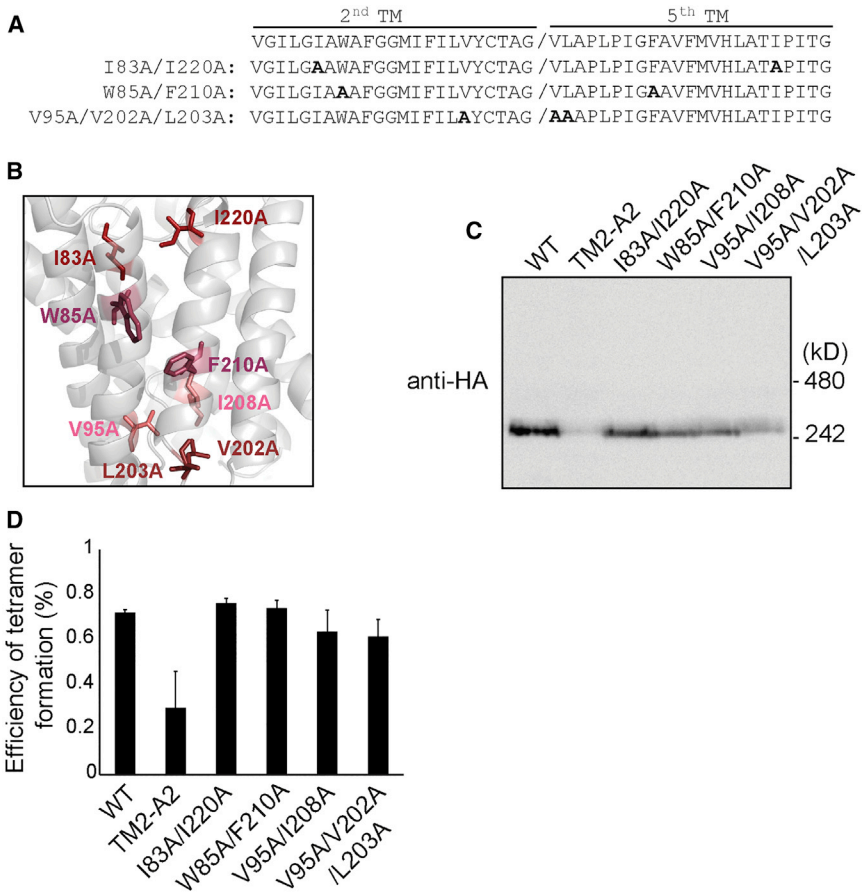

Figure 4. Alanine Substitution in TM Residues Predicted as Interaction Partners in TM2 and TM5 Do Not Affect AtPIP2;1 Tetramer Formation.

(A) Sequences of alanine substitution mutants in TM2 and TM5. Residues predicted to have potential inter-TM interactions between TM2 and TM5 were substituted with alanines. Bold letters indicate alanine substitution.

(B) Model structure showing residues predicted to have inter-TM interactions between TM2 and TM5. The amino acid residues substituted with alanine are indicated in red.

(C) Effect of alanine substitution mutations on tetramer formation. Protoplasts were transformed with the indicated constructs, and protein extracts were separated by BN–PAGE, followed by western blot analysis using anti-HA antibody. WT, AtPIP2;1:HA.

(D) Quantification of tetramer formation efficiency. To quantify the efficiency of tetramer formation, the tetramer band intensity was measured using LAS3000 software. The efficiency of tetramer assembly is expressed as the relative value over total expressed proteins. The values are means with SE (n = 2).

AtPIP2;1:HA. Dimers are produced by a disulfide bond between conserved cysteine residues (Supplemental Figure 5) when AQPs are assembled into tetramers (Bienert et al., 2012). In these mutants, the disulfide bond was not present or was more easily broken by β-mercaptoethanol in the solubilization buffer due to a conformational change introduced by the mutations. These results suggest that the mutations affect tetramer assembly. We further examined the nature of these AtPIP2;1 and mutant complexes. We subjected V41A/E44A:HA and WT AtPIP2;1:HA to chemical crosslinking using the crosslinking agent disuccinimidyl suberate (DSS) after separating these proteins on a blue native gel. The crosslinked proteins were then analyzed by SDS–PAGE in the second dimension (Figure 5E). The second dimensional SDS–PAGE showed that the tetramer band of WT proteins in the blue native gel produced four bands corresponding to the monomer, dimer, trimer, and tetramer forms of AtPIP2;1, confirming the subunit composition of the AtPIP2;1 tetramers. Similarly, the multiple discrete and smeared bands of V41A/E44A above the tetramer also produced protein bands corresponding to the monomer, dimer, trimer, and tetramer forms of AtPIP2;1. Furthermore, a band at the pentamer position was also produced, with a smeared pattern above the pentamer. Bands higher than the pentamer were not discernable due to limited resolution (Figure 5E). These results suggest that the multiple discrete and smeared bands above the tetramer were oligomeric complexes of AtPIP2;1 with more than four subunits rather than non-specific aggregates. In these crosslinking experiments, we cannot exclude the possibility that the DSS treatment might also cause crosslinking with native PIPs in protoplasts, and detection with HA might include crosslinked native AtPIP2;1 or even PIP1s that form heterotetramers with AtPIP2;1. These results suggest that V41, E44, F51, and L52 play a crucial role in the assembly of AtPIP2;1 tetramers.

Next, we identified amino acid residues in TM2 by generating four double mutants, i.e., I81A/W85A, F87A/I91A, F92A/I93A, and V95A/Y96A (Figure 6A). These mutants were tagged with HA at the C terminus and expressed in protoplasts. The constructs were analyzed by BN–PAGE, followed by western blot using anti-HA antibody (Figure 6C). Of these mutants, F87A/I91A:HA showed a severe defect in tetramer assembly, with less than 27% efficiency, a level similar to that of two TM1 mutants, V41A/E44A:HA and F51A/L52A:HA (Figure 6E). In addition, two mutants, F92A/I93A:HA and V95A/Y96A:HA, also showed a significant defect in tetramer assembly, with 40%–55% efficiency (Figure 6E). These results indicate that F87, I91, F92, I93, V95, and Y96 in TM2 play a crucial role in AtPIP2;1 tetramer assembly.

We generated three double substitution mutants of TM4, including I175A/I176A:HA, T178A/F179A:HA, and V182A/Y183A:HA (Supplemental Figure 6). V185A/F186A:HA was excluded from analysis due to its low expression levels. However, the other two mutants did not have significant effects on tetramer levels (Supplemental Figure 6).

We generated six double substitution mutants of TM5, including P205A/L206A:HA, P207A/I208A:HA, F210A/V212A:HA, F213A/M214A:HA, H216A/L217A:HA, and L217A/I220A:HA (Figure 6B). Of these mutants, F213A/M214A:HA was excluded

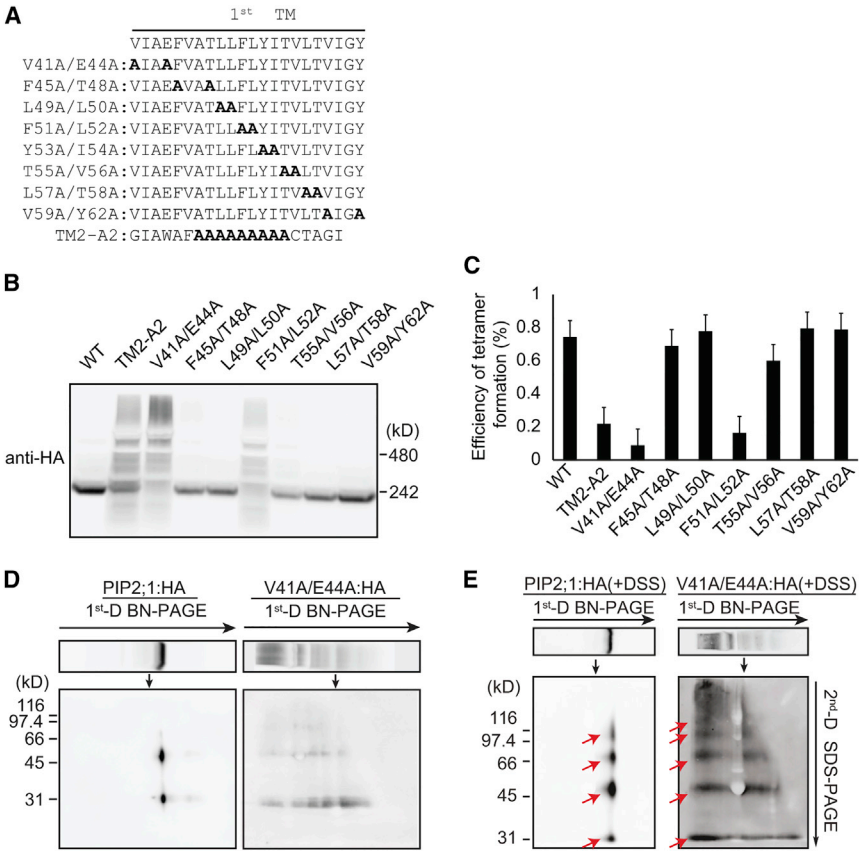

Figure 5. Certain Double Alanine Substitution Mutations in TM1 Cause Failure to Form Tetrameric AtPIP2;1 Complexes.

(A) Sequences of alanine substitution mutants in TM1. The two nearest residues predicted to have potential inter-TM interactions within a monomer were sequentially substituted with alanines throughout the entire sequence of TM1. Bold letters indicate alanine substitution.

(B) Effect of double alanine substitution TM1 mutants on tetramer formation. Protoplasts were transformed with the indicated constructs, and protein extracts were separated by BN–PAGE, followed by western blot analysis using an anti-HA antibody. WT, AtPIP2;1:HA.

(C) Quantification of tetramer formation efficiency. To quantify the efficiency of tetramer formation, the tetramer band intensity was measured using LAS3000 software. The efficiency of tetramer assembly is expressed as the relative value over total expressed proteins. The values are means with SE (n = 2).

(D and E) Two-dimensional gel electrophoresis of WT and V41A/E44A proteins. Protein extracts from protoplasts transformed with WT (*AtPIP2;1:HA*) and *V41A/E44A:HA* were separated by blue native gel electrophoresis. Subsequently, the blue native gel was subjected to SDS–PAGE in the second dimension with **(D)** or without **(E)** chemical crosslinking using DSS. Red arrows indicate various oligomeric forms of AtPIP2;1.

from analysis due to its low expression levels. Of the five remaining mutants, only H216A/L217A:HA showed a significant decrease in tetramer production, instead producing a multiple discrete and smeared banding pattern above the tetramer band (Figure 6D), indicating that H216 and L217 play a critical role in the formation of AtPIP2;1 tetramers. Y53A/I54A:HA, V185A/F186A:HA, and F213A/M214A:HA were expressed at extremely low levels. We treated the protoplasts with MG132, an inhibitor of the proteasome (Supplemental Figure 7). This treatment did not affect the levels of these mutant proteins, indicating that these mutants have a defect in transcription or translation.

Residues Important for Tetramer Formation Are Involved in Inter-TM Helical Interactions within Monomers

To elucidate the role played by these residues in the formation of AtPIP2;1 tetramers, we examined their interactions in detail, including the number of van der Waals interactions and the types of interactions and interaction partners, using the model structure of AtPIP2;1 (Figure 2). We particularly focused on the interactions between TM helices because these residues should greatly affect the conformation of TM helices in the membrane, thereby playing a crucial role in tetramer formation. We used Sting software (Neshich et al., 2005) to identify the residues of neighboring TM helices that may interact with the residues identified as crucial for the formation of AtPIP2;1 tetramers. These interactions are shown in Figure 7. A pair of critical TM1 residues, V41 and E44, was predicted to interact with three residues in neighboring TM3: V41 with L127 and A131 in TM3, and E44 with Q132 in TM3 (Figure 7A). In another pair of critical TM1 residues (F51 and L52), F51 was predicted to interact with three residues (F87, I91, and L94) in TM2, and L52 in TM1 was predicted to interact with V140 in TM3 (Figure 7B). Thus, residues V41, E44, F51, and L52 in TM1 constitute an inter-TM network of three TM helices, TM3-TM1-TM2. Of these residues, F87 and I91 in TM2 were identified by mutagenesis (Figure 7B), confirming that our prediction correctly identified important residues involved in AtPIP2;1 tetramer assembly. F87 and I91, which are involved in the interaction with TM1 on one side, were also predicted to interact with I208, V212, and H216 in TM5 on the other side (Figure 7C). Thus, F87 and I91 are located in the center of a long TM helical interaction network consisting of TM3-TM1-TM2-TM5. Of the residues predicted to be interacting partners of residues F87 and I91 in TM2, F51 in TM1 and H216 in TM5 were identified as crucial residues in tetramer assembly by mutagenic analysis (Figures 5B, 6C, and 6D). Finally, a pair of critical TM5 residues, H216 and L217, was predicted to interact with F87 and A84 in TM2, respectively (Figure 7D). Of these predicted residues, F87 in TM2 was identified by mutagenic analysis. Thus, we identified 17 interactions that occur within monomers (Figure 7, Table 1), including 14 hydrophobic interactions, two aromatic stacking interactions (F87/F51 and F87/H216), and one hydrogen bonding (E44/Q132).

In addition to the inter-TM interactions within monomers, Sting software predicted that the critical residues in TM helices are also involved in the following interactions between monomers (Figure 8): Y96 at the end of TM2 α helix with P207 at the cytosolic end of TM5 (Figure 8A); F92 and I93 with F210 at the

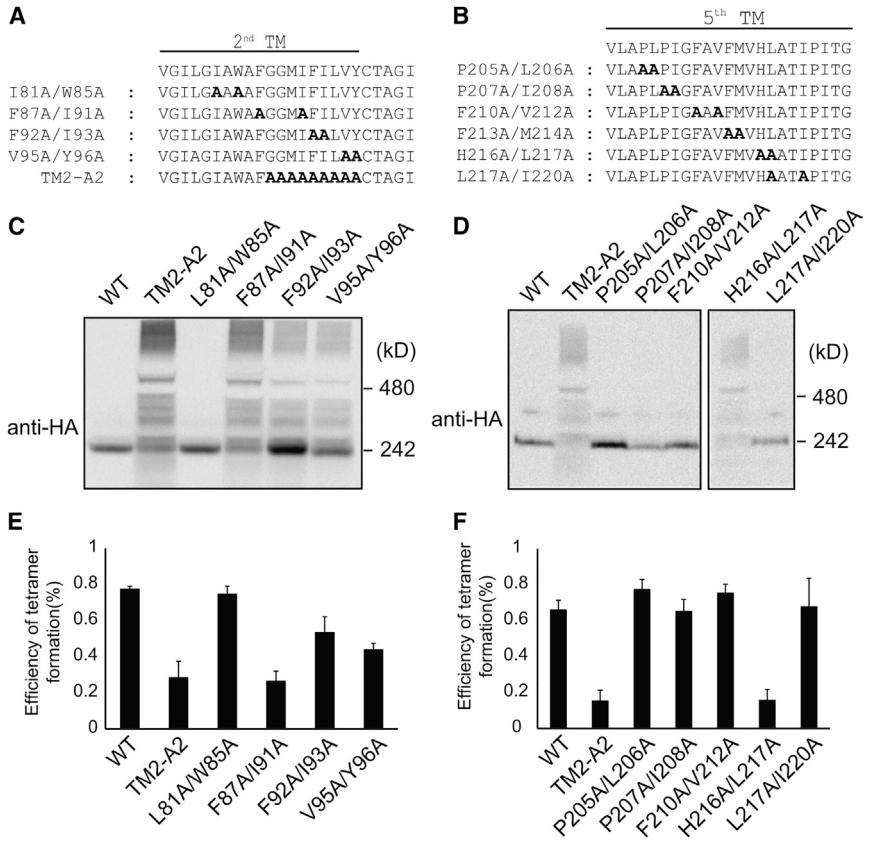

Figure 6. TM2 and TM5 Contain Residues Critical for Formation of the Tetrameric AtPIP2;1 Complex.

(A and B) Amino acid sequences of double alanine substitution mutants of TM2 **(A)** and TM5 **(B)**. Residues substituted with alanines are indicated by bold letters.

(C) Effect of double alanine substitutions in TM2 on tetramer formation. Protein extracts from protoplasts transformed with the indicated constructs were separated by BN–PAGE and analyzed by western blotting using anti-HA antibody. WT, AtPIP2;1:HA.

(D) Effect of double alanine substitutions in TM5 on tetramer formation. Protein extracts from protoplasts transformed with the indicated constructs were separated by BN–PAGE and analyzed by western blotting using anti-HA antibody. WT, AtPIP2;1:HA.

(E and F) Quantification of tetramer formation efficiency. To quantify the efficiency of tetramer formation, the tetramer band intensity was measured using LAS3000 software. The efficiency of tetramer assembly is expressed as the relative value over total expressed proteins. The values are means with SE (n = 3).

cytosolic side (Figure 8B); and L217 of TM5 with T58 of TM1 at the luminal end (Figure 8C). These five interactions between monomers include one aromatic and four hydrophobic interactions. Intriguingly, of the residues identified to have inter-TM interactions between monomers, T58, P207, and F210 did not have a significant effect on tetramer assembly when substituted with alanines (Figures 5B and 6D). One possible explanation is that elimination of a single interaction between monomers may not have a noticeable effect on tetramer assembly. Accordingly, we generated two double mutants, F92A/Y96A:HA and P207A/F210A:HA (Supplemental Figure 8). Both F92A/Y96A:HA and P207A/F210A:HA produced significant amounts of high molecular weight complexes that migrated above the tetramer, although the majority of proteins still produced the tetramer band, indicating that these residues contribute to tetramer assembly to a certain degree (Supplemental Figure 8). These results raise the possibility that inter-TM interactions between monomers function cooperatively with interactions within monomers to induce a specific conformation of TM helices, particularly TM5, thereby contributing to AtPIP2;1 tetramer assembly.

Formation of AtPIP2;1 Tetramers Is Important for Trafficking of AtPIP2;1 to the PM

AtPIP2;1 is a PM protein. Thus, we examined the relationship between tetramer formation and trafficking to the PM. It is generally accepted that oligomerization of AQPs occurs at the ER (Zelazny et al., 2007; Sorieul et al., 2011). Three double substitution mutants (F87A/I91A, V95A/Y96A, and H216A/L217A) showing a defect in tetramer formation in the complex, as well as WT AtPIP2;1, were fused to mCherry at the C terminus. These constructs were transferred to a binary vector and transiently expressed in leaf tissues by *Agrobacterium*-mediated infiltration. Transgenic GFP:HDEL was used as a marker for the ER. WT AtPIP2;1:mCherry (WT:mCherry) appeared to localize to the PM (Figure 9A). Consistent with this notion, this protein did not co-localize with GFP:HDEL (Figure 9A). By contrast, the three mutant fusion proteins, F87A/I91A:mCherry, V95A/Y96A:mCherry, and H216A/L217A:mCherry, produced a different pattern from that of WT:mCherry. Moreover, these mutants largely co-localized with GFP:HDEL (Figure 9A), indicating that they localized to the ER. To confirm their localization, we compared the signal intensities of these mutants and WT:mCherry proteins along the line that crosses the entire epidermal cell with that of the ER. The signal intensity profiles of these three mCherry-tagged mutants closely overlapped with that of GFP:HDEL, while that of WT:mCherry did not, confirming that these mutants localized to the ER. In addition, H216A/L217A:mCherry produced punctate signals. To define the localization of the punctate signals, we expressed *H216A/L217A:mCherry* in transgenic plants expressing *ST:GFP* (Figure 9B). H216A/L217A:mCherry did not co-localize with ST:GFP, indicating that H216A/L217A:mCherry did not localize to the Golgi. These results suggest that tetramer formation in the ER is a prerequisite for trafficking to the PM.

Formation of AtPIP2;1 Tetramers Is Important for Water Permeability

Formation of AQP tetramers is a prerequisite for water permeability (Duchesne et al., 2001). We examined whether a defect in tetramer assembly, and thus a defect in trafficking to the PM, would affect water permeability *in vivo*. In previous studies, plant proteins functioned properly in *Xenopus* oocytes (Fetter

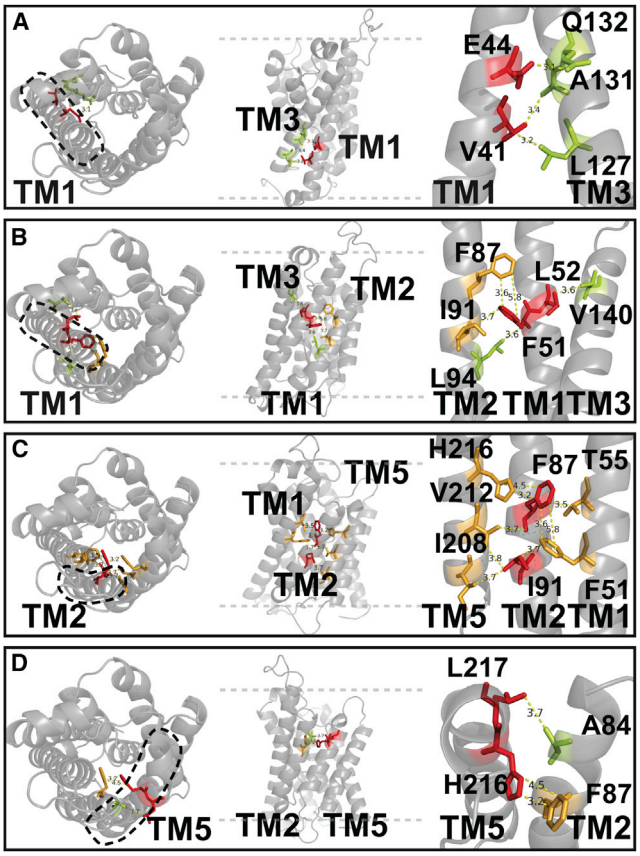

Figure 7. The Majority of Residues Critical for the Formation of AtPIP2;1 Tetramers Are Involved in Inter-TM Interactions within Monomers.

(A) Interaction network of E44 and V41. E44 and V41 residues in TM1 (left panel) interact with three residues in TM3 (middle panel). A close-up view of the interaction network generated by E44 and V41 is shown in the right panel.

(B) Interaction networks of F51 and L52. F51 and L52 residues in TM1 (left panel) interact with three residues in TM2 and one residue in TM3 (middle panel). A close-up view of the interaction networks involving F51 and L52 is shown in the right panel.

(C) Interaction networks of F87 and I91. F87 and I91 residues in TM2 (left panel) interact with two residues in TM1 and three residues in TM5 (middle panel). A close-up view of the interaction networks involving F87 and I91 is shown in the right panel.

(D) Interaction network of H216 and L217. H216 and L217 residues in TM5 (left panel) interact with two residues in TM2 (middle panel). A close-up view of the interaction network involving H216 and L217 is shown in the right panel. The interaction partners of residues found to play a crucial role in tetramer assembly by mutagenesis were predicted with Sting software using the model structure of AtPIP2;1.

Residues in red, green, and orange were identified experimentally, by prediction, and both experimentally and by prediction, respectively. Yellow dashed lines indicate inter-TM interactions between residues. Numbers above dashed lines represent distance in Å.

Pos1	Residue1	Distance	Resdue2	Pos2
Interactions within monomers				
41	V	3.21	L	127
41	V	3.426	A	131
44	E	3.142	Q	132
51	F	3.647	F	87
51	F	5.834	F	87
51	F	3.722	I	91
51	F	3.56	L	94
52	L	3.613	V	140
55	T	3.482	F	87
84	A	3.658	L	217
87	F	3.726	V	212
87	F	3.232	H	216
87	F	4.53	H	216
91	I	3.737	I	208
91	I	3.765	V	212
92	F	3.674	P	205
92	F	3.543	L	206
Interactions between monomers				
58	T	3.776	L	217
92	F	3.707	F	210
92	F	5.174	F	210
93	I	3.778	F	210
96	Y	3.576	P	207

Table 1. Amino Acid Residues Involved in Inter-TM Interactions with the Residues Identified by Double Alanine Substitution Mutagenesis.

Amino acid residues having inter-TM interactions with the residues found to play a critical role in tetramer formation were predicted from the model structure of AtPIP2;1 using Sting software.

et al., 2004; Zelazny et al., 2007; Bienert et al., 2012; Jozefkowicz et al., 2013). We therefore measured the water permeability coefficient (P_f) of WT AtPIP2;1 and V41A/E44A in *Xenopus* oocytes (Figure 10A). The tetramer assembly efficiency of V41A/E44A was approximately 10% in protoplasts (Figure 5). We introduced WT *AtPIP2;1* and *V41A/E44A* transcript in oocytes, and investigated the expression of these proteins by western blot analysis using anti-HA antibody (Figure 10B). Both WT *AtPIP2;1* and *V41A/E44A* were expressed at equal levels. Next, we examined the water permeability in oocytes 72 h after injection of transcripts. Both WT AtPIP2;1 and V41A/E44A showed an increase in water permeability compared with the water control. However, the P_f value of V41A/E44A was lower than that of WT AtPIP2;1, indicating that V41A/E44A had defective water permeability to a certain degree. However, V41A/E44A still showed significant levels of water permeability, perhaps because the mutant protein still formed tetramers.

DISCUSSION

In this study, we focused on two aspects of AtPIP2;1 biogenesis, i.e., tetramer assembly and trafficking to the PM. Moreover, we examined the relationship between tetramer assembly and water permeability of AtPIP2;1 in *Xenopus* oocytes. We identified many residues in TM helices of AtPIP2;1 that play crucial roles in tetramer formation via interactions between TM helices (Figure 11A). There are two different types of these interactions,

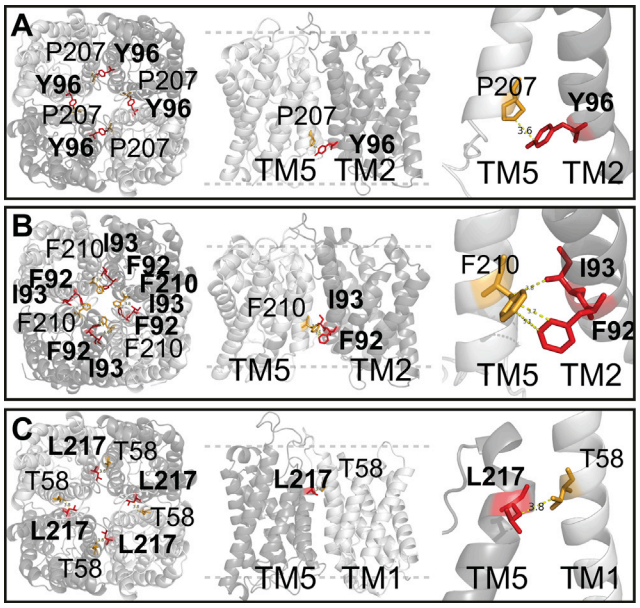

Figure 8. A Minor Portion of Residues Crucial for Tetramer Formation Are Involved in Inter-TM Interactions between Monomers.

(A) Y96 interacts with P207 in the tetramer (left panel). Y96 is located at the end of TM2 (middle panel). A close-up view of the Y96 and P207 interaction network is shown in the right panel. The inter-TM interactions between monomers are shown in detail in the AtPIP2;1 model structure. The interaction partners of those identified by mutagenesis were predicted using Sting software.

(B) I93 and F92 interact with F210 in the tetramer (left panel). I93 and F92 are located at the end of TM2 (middle panel). A close-up view of the I93 and F92 interaction network is shown in the right panel.

(C) L217 interacts with T58 in the tetramer (left panel). L217 is located at the end of TM5 (middle panel). A close-up view of the L217 and T58 interaction network is shown in the right panel.

Residues in red were found by mutagenesis to play a critical role in protomer number determination. Residues in orange were identified by both mutagenesis and prediction. Yellow dashed lines indicate inter-TM interactions between monomers. Numbers above dashed lines indicate the distance between residues in Å.

i.e., those occurring within monomers and those occurring between monomers; the majority of these interactions occur within monomers. The results obtained by mutagenic analysis followed by modeling suggest that the two different types of interactions between TM helices constitute part of the structural requirement for tetramer formation. In fact, TM conformation may play a key role in determining the overall structure of a protein complex, as is the case for AQPs, which are membrane proteins largely composed of many TM helices. Inter-TM interactions occurring within monomers may be particularly crucial for the conformation of monomers. Previous studies have also demonstrated the importance of the interactions between TM helices within monomers (Haeger et al., 2010). For example, interactions between TM2 and TM5 within a monomer contribute to pore formation in the water channel (Törnroth-Horsefield et al., 2006; Yu et al., 2006). However, the TM residues involved in the inter-TM interactions identified in the present study may be different from those involved in pore formation because we specifically identified the residues whose mutation resulted in the failure to produce tetramers. In fact, alanine substitution of these residues in pairs resulted in the production of multiple complexes with molecular weights higher than that of the tetramer. Moreover, one of these mutants with a defect in tetramer assembly exhibited reduced levels of water permeability in *Xenopus* oocytes (Figure 10).

Our combined experimental approaches, involving mutagenesis, followed by expression in protoplasts and AtPIP2;1 model structure-based prediction using software, provided a detailed picture of the possible interactions between TM helices. The inter-TM interactions that occur within monomers constitute three interaction networks, including one long interaction network consisting of TM3-TM1-TM2-TM5 and two short networks, TM1-TM3 and TM2-TM5. AQPs are thought to have evolved through gene duplication (Wistow et al., 1991; Murata et al., 2000). Thus, the N-terminal segment containing TM1 to TM3 may be equivalent to the C-terminal segment containing TM4 to TM6. However, for a single polypeptide such as AtPIP2;1, after the fusion of two fragments, each of these six TM helices will have its own specific conformation, including a specific tilting angle in the membrane, a specific interaction between TM helices, and so on, as revealed by its three-dimensional structure (Törnroth-Horsefield et al., 2006). These inter-TM interactions within a monomer may greatly contribute to inducing the specific conformation of TM helices. Thus, as shown with the alanine substitution mutants, without these inter-TM interactions among four TM helices (TM1, TM2, TM3, and TM5), there may be a high degree of freedom regarding the conformation of these TM helices within a monomer, including the tilting angle in the membrane and the interactions between TM helices, which in turn allows the mutants to assemble into multiple oligomeric complexes. Supporting this idea is the observation that bacterial formate transporter FocA assembles into pentamers even though it has a monomer structure highly similar to that of AtPIP2;1 (Figure 11B). Despite their lack of primary sequence similarity, AQP and FocA have only slight differences in TM conformations; TM helices of FocA are slightly more tilted than those of AtPIP2;1 (Figure 11B). As a result, the FocA monomer appears to be more constricted than the AQP1 monomer (Wang et al., 2009; Theobald and Miller, 2010; Waight et al., 2010). Thus, if there are slight changes in tilting in its TM helices, AtPIP2;1 can assemble into oligomeric complexes with different numbers of subunits.

Another type of inter-TM interaction is the one that occurs between monomers. These interactions may also contribute to tetramer formation, since eliminating these interactions also resulted in the formation of multiple high molecular weight complexes. However, the amount of mutant protein in high molecular weight complexes was much lower than that resulting from the elimination of interactions within monomers. These results raise the possibility that inter-TM interactions between monomers also contribute to tetramer formation, but to a much lesser degree than inter-TM interactions within monomers. One possible way these interactions may contribute to tetramer formation is that they may also be involved in inducing a specific TM helix conformation in a monomer that allows AtPIP2;1 to only have four subunits in the complex. Intriguingly, two of these interactions occur at the cytosolic end of the TM helix, specifically at the kink position of TM2, and the third occurs at the luminal end, thereby being ideally positioned to

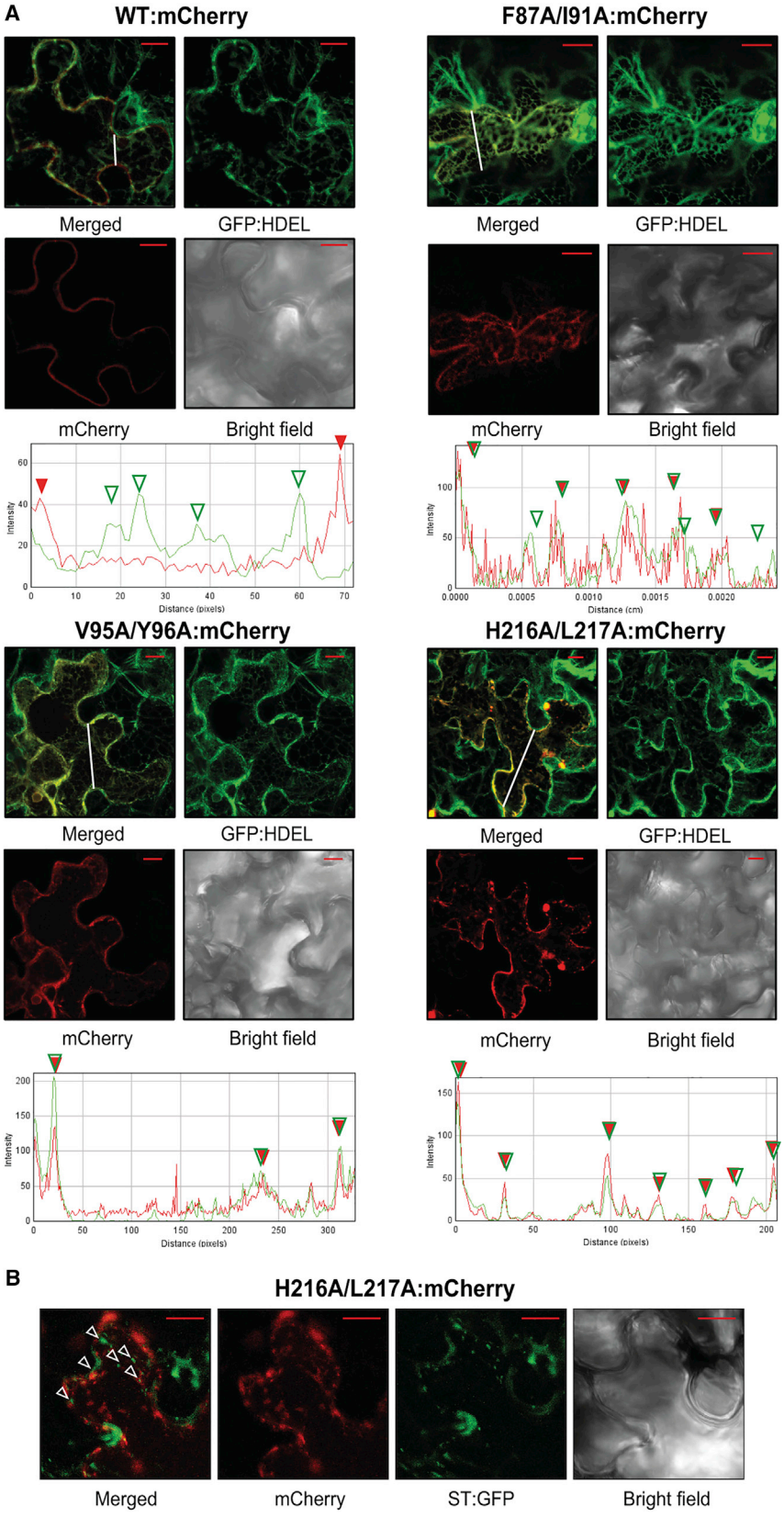

Figure 9. Tetrameric Assembly of AtPIP2;1 Is Required for Its Trafficking from the ER to the Plasma Membrane. The graph shows the intensity of GFP and mCherry signals along the white line. The peaks of GFP and mCherry signals are indicated by green and red triangles, respectively.

(A) Localization of mutant constructs. Leaves of GFP:HDEL transgenic plants were infiltrated with *Agrobacterium tumefaciens* carrying mCherry fusion constructs of *F87A/I91A*, *V95A/Y96A*, or *H216A/L217A*. The leaf tissues were examined by confocal laser scanning microscopy. WT:mcherry, AtPIP2;1:mcherry. Scale bars, 10 μm.

(B) Lack of colocalization of H216A/L217A:mCherry with ST:GFP. Transgenic plants expressing ST:GFP were infiltrated with *Agrobacterium tumefaciens* carrying an mCherry fusion construct of *H216A/L217A:mCherry*. The arrowheads indicate the punctate signals of H216A/L217A:mCherry.

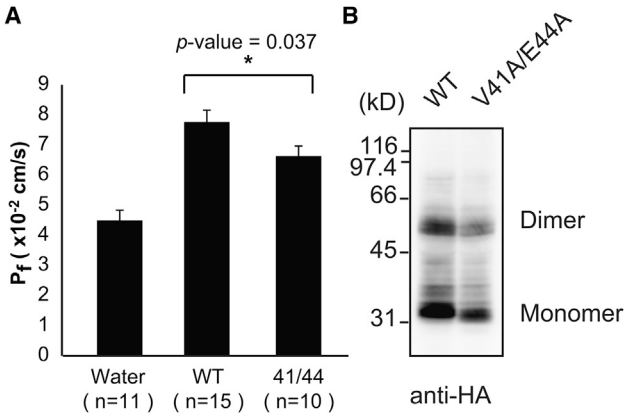

Figure 10. The V41A/E44A Mutant Shows a Defect in Water Permeability *In Vivo*.

(A) Water permeability coefficients. The water permeability coefficients were calculated according to the formula described in the Methods. Data were analyzed by Student's *t*-test, $P = 0.037$.

(B) Expression of AtPIP2;1 and V41A/E44A in oocytes. The expression of WT AtPIP2;1:HA and mutant V41A/E44A:HA was detected by western blot using anti-HA antibody.

induce specific TM helix conformations, particularly for TM5. These results raise the possibility that a certain specific conformation of TM helices is not intrinsically built into monomers but is achieved only through interactions between monomers. Structural changes during tetramer formation are thought to have important implications; AQPs are active as water channels only when they are in tetramer form, although monomers contain water channel pores (Duchesne et al., 2002; Buck et al., 2007). Thus, the activation of AQPs may occur through the conformational change induced by tetramerization. Moreover, these inter-TM interactions within and between monomers are intimately connected. Of the residues involved in the inter-TM interaction between monomers, L217 in TM5 is also involved in inter-TM interactions within monomers, suggesting that inter-TM interactions between monomers work cooperatively with those within monomers to induce specific TM conformations, thereby aiding in tetramer formation (Figure 7).

Another important aspect of AtPIP2;1 biogenesis is its trafficking to the PM. In plant cells, AQP homologs were identified in multiple organelle membranes, including the ER, PM, tonoplast, and protein storage vacuole (Hachez et al., 2013; Luu and Maurel, 2013). Thus, biogenesis of these AQP homologs to their final destination is likely controlled at two different levels: specificity determination and their assembly into tetramers. Previous studies identified a sequence motif at the N-terminal region of AtPIP2;1 required for its ER exit in plant cells (Sorieul et al., 2011). In maize, the trafficking behaviors of two PIP isoforms differ. ZmPIP2;5 alone is successfully targeted to the PM, whereas singly expressed ZmPIP1;2 is retained in the ER. In ZmPIP2s, the LxxxA motif of TM3 acts as a signal for trafficking to the PM. By contrast, this motif is absent in ZmPIP1;2 (Chevalier et al., 2014). Coexpression of ZmPIP1;2 with ZmPIP2;5 results in its targeting to the PM, suggesting that hetero-complex formation of ZmPIP1;2 with ZmPIP2;5 at the ER is required for trafficking of ZmPIP1;2 to the PM (Zelazny et al., 2007; Sorieul et al., 2011). The LxxxA motif is conserved in AtPIP2;1 (Supplemental Figure 5). Intriguingly, V41 and E44 were predicted to interact with L127 and A131, the two critical residues in the LxxxA motif. Thus, perhaps this motif plays a role in trafficking via tetrameric assembly of AtPIP2;1. The importance of certain residues in TM helices was also demonstrated in human AQP2; single-point mutations in TM2 and TM3 of human AQP2, which cause congenital nephrogenic diabetes insipidus, also result in protein accumulation in the ER.

Based on these results, we propose that inter-TM interactions within and between monomers largely mediated by hydrophobic and aromatic residues of TM helices play a crucial role in the formation of the tetrameric AtPIP2;1 complex. This finding is in contrast to the previous study showing that asparagine (N49), lysine (K51), and aspartate (D185) of human AQP1 play a crucial role in oligomerization. Thus, our study raises the possibility that the oligomerization mechanism of AQPs may depend on specific isoforms of AQPs. In addition, our study provides evidence that tetramer formation is critical for trafficking from the ER to the PM and confirms that tetramer formation is crucial for water permeability.

METHODS

Plant Materials and Growth Conditions

Arabidopsis thaliana (Col-0) plants were grown on Gamborg's B5 plates in a growth chamber at 40% relative humidity, 22°C, under a 16-h light/8-h dark cycle. Leaf tissues were harvested from 2- to 3-week-old plants and used for protoplast isolation.

Plasmid Construction

To generate AtPIP2;1:HA, cDNA was amplified by PCR using primers AtPIP2;1-XhoI-F and AtPIP2;1-BamHI-B (Supplemental Table 1), digested with *Xho* I and *Bam* H1, and inserted between the 35S CaMV promoter and the Nos-terminator of an HA-tagging vector digested with *Sal* I/*Bam* HI. Alanine substitution mutations in the TM helices were introduced by two rounds of sequential PCR using two complementary forward and reverse primers (Supplemental Table 1). First-round PCR was performed to generate 5′ and 3′ fragments of all mutants using AtPIP2;1:HA as a template. The 5′ fragment of each mutant was amplified using the common cauliflower mosaic virus (CaMV)-5′ primer and a mutant-specific reverse primer. The 3′ fragment of each mutant was amplified using a mutant-specific forward primer and the common Nos-terminator primer. Second-round PCR was performed using the 5′ and 3′ PCR products of the first-round PCR as a template with CaMV-5′ and Nos-terminator primers. Finally, the second-round PCR products were subcloned into an expression vector and their sequences were confirmed by nucleotide sequencing.

Homology Modeling of AtPIP2;1

Modeling of AtPIP2;1 was carried out using software housed in the Swiss Model web server. AtPIP2;1 has a high degree of sequence similarity (identity, 75.261%) to SoPIP2;1 (3CN6). The van der Waals interactions were measured based on distance. Hydrophobic interactions, aromatic stacking, and hydrogen bonding between residues in the TM helices were analyzed using Sting software (Neshich et al., 2005).

Structural Alignment of AtPIP2;1 and FocA

Structural alignment of AtPIP2;1 and FocA (3KLY) was performed using the program Coot (Emsley et al., 2010). The SSM (overlay protein structures using secondary structure) method was used for alignment (Emsley et al., 2010).

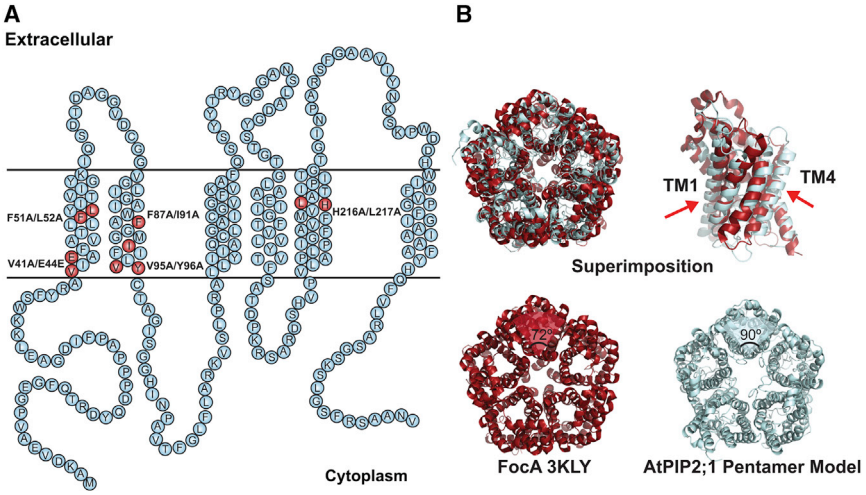

Figure 11. Schematic Representation of the Locations of TM Residues that Are Crucial for Tetrameric Assembly of AtPIP2;1.

(A) Schematic diagram showing the primary sequence and membrane topology of AtPIP2;1 at the plasma membrane. The TM residues found to play a crucial role in tetramer assembly by mutagenesis are shown in red.

(B) Superimposed structures of AtPIP2;1 and FocA.

PEG-Mediated Transformation and Western Blot Analysis of Protein Extracts

Isolation of *Arabidopsis* protoplast was performed as described previously (Jin et al., 2001). Briefly, 2- to 3-week-old *Arabidopsis* plants were harvested and incubated in enzyme solution (0.25% Macerozyme [Yakult Honsha, Tokyo, Japan] R-10, 1.0% cellulase [Yakult Honsha] R-10, 400 mM mannitol, 8 mM $CaCl_2$, and 5 mM Mes-KOH [pH 5.6]) at 22°C for 5–8 h with gentle shaking (50–75 rpm) in the dark. After incubation, the protoplast suspension was filtered through 100 μm mesh and the protoplasts were harvested by centrifugation at 46 *g* for 5 min. After discarding the enzyme solution, the pelleted protoplasts were resuspended in 5–10 ml of W5 solution (154 mM NaCl, 125 mM $CaCl_2$, 5 mM KCl, 5 mM glucose, and 1.5 mM Mes-KOH [pH 5.6]), overlaid on top of 20 ml of 21% sucrose, and centrifuged for 10 min at 78 *g*. The intact protoplasts at the interface and on top were transferred to a new conical tube containing 20 ml of W5 solution. The protoplasts were again pelleted by centrifugation at 55 *g* for 5 min and resuspended in 20 ml of W5 solution. The protoplasts were stored at 4°C and used within 6 h.

For transient expression analysis, plasmid DNA was introduced into protoplasts isolated from leaf tissues of 2- to 3-week-old *Arabidopsis* plants using PEG-mediated transformation (Kim et al., 2001). The transformed protoplasts were pelleted at the appropriate time points after transformation and resuspended in denaturation buffer (2.5% SDS and 2% β-mercaptoethanol). The resuspended samples were incubated at 65°C for 15 min and the debris was removed by centrifugation. Gel-loading buffer (50 mM Tris-Cl [pH 6.8], 0.1 M DTT, 2% SDS, 0.01% bromophenol blue, and 10% glycerol) was added to the supernatant for SDS–PAGE and western blot analysis. Immunoblot images were obtained using an LAS3000 image capture system (FujiFilm, Japan).

BN–PAGE Analysis

BN–PAGE analysis was performed as described previously (Kikuchi et al., 2006). Protoplasts were resuspended in solubilization buffer (50 mM Bis-Tris-HCl [pH 7.0], 0.5 M aminocaproic acid, 10% w/v glycerol, 2% n-Dodecyl β-D-maltoside, and 1% protease inhibitor cocktail). The resuspended pellets were incubated on ice for 10 min and centrifuged at 20 000 *g*. Insoluble materials were removed by ultracentrifugation at 100 000 *g* for 10 min. The supernatant was combined with Coomassie brilliant blue G-250, and the samples were loaded onto a 4%–16% gradient gel (Native PAGE Novex 4%–16% Bis-Tris Gel; Invitrogen, Carlsbad, CA, USA). The cathode tank buffer contained 50 mM Tricine/15 mM Bis-Tris (pH 7.0), and 0.02% CBB-G-250, and the anode tank buffer contained 50 mM Bis-Tris (pH 7.0). Gel electrophoresis was performed at 4°C. Western blot analysis was performed using anti-HA antibody.

Two-Dimensional Gel Electrophoresis

After BN–PAGE, each lane of the gel was sliced into a strip and equilibrated in denaturation buffer (3.3% [w/v] SDS and 4% [v/v] 2-mercaptoethanol in 65 mM Tris-HCl [pH 6.8]) for 30 min at 37°C. The gel strip was placed horizontally onto an 8% SDS–polyacrylamide gel. After SDS–PAGE, the proteins were analyzed by western blotting using an anti-HA antibody.

Chemical Crosslinking of AtPIP2;1 Proteins and MG132 Treatment

Chemical crosslinking experiments were performed using DSS (Thermo Scientific Pierce, Rockford, IL, USA) as a crosslinking reagent. After BN–PAGE, a sliced strip containing each lane of the blue native polyacrylamide gel was incubated for 30 min in 1 mM DSS and resolved in PBS buffer at room temperature. The crosslinking reaction was quenched with stop solution (50 mM Tris-HCl, pH 7.0) for 15 min. Treatment of protoplasts with MG132 was performed as described previously (Lee et al., 2009).

Agrobacterium-Mediated Infiltration and Image Analysis

DNA constructs in the pBIB binary vector (Becker, 1990) were transformed into *Agrobacterium tumefaciens*. The Agrobacteria were cultured overnight at 28°C in 5 ml of Luria-Bertani (LB) medium containing 50 mg/ml rifampicin and 50 mg/ml kanamycin. The overnight culture (0.5 ml) was inoculated into 5 ml of fresh LB medium containing 50 mg/ml kanamycin and grown to an optical density at 600 nm (OD_{600}) of 1–2. The bacteria were harvested by centrifugation at 3000 *g* and resuspended in induction medium (50 mM MES [pH 5.6], 0.5% glucose, 2 mM $NaH_2PO_4 \cdot 2H_2O$, 200 mM acetosyringone, and 1× AB salts [20× AB salts: 20 g/l NH_4Cl, 6 g/l $MgSO_4 \cdot 7H_2O$, 3 g/l KCl, 0.2 g/l $CaCl_2 \cdot 2H_2O$, and 50 mg/l $FeSO_4 \cdot 7H_2O$]) to OD_{600} - 0.2, followed by incubation at 28°C for 6 h (Yang et al., 2000). After incubation, the culture was diluted with induction medium to OD_{600} = 0.2 and injected into leaves using a 1 ml syringe without a needle as described previously (Wroblewski et al., 2005). Agro-infiltrated plants were incubated in the dark for 1 day, and infected leaves were observed under a confocal laser scanning microscope (Carl Zeiss LSM510META system) at 3 days after infiltration. The excitation wavelengths/emission filters were 488 nm (argon-ion laser)/505 to 530 nm band-pass for GFP, 543 nm (HeNe laser)/560 nm long-pass for chlorophyll autofluorescence, and 543 nm/560 to 615 nm band-pass for mCherry. The images are presented in pseudo color.

cRNA Synthesis *In Vitro*

Capped cRNAs encoding *AtPIP2;1:HA* and *V41A/E44A:HA* were synthesized *in vitro* using an mMESSAGE mMACHINE T7 Capped RNA Transcription Kit (Ambion). The pGEMHE vector carrying the corresponding sequence as template was linearized by PCR.

Water Permeability Measurement in *Xenopus* Oocytes

Defoliculated *Xenopus* oocytes (stages 5 and 6) were injected with 20 ng/50 nl cRNA. Injected oocytes were incubated for 72 h at 18°C in Barth's buffer (88 mM NaCl, 1 mM KCl, 0.82 mM $MgSO_4$,

0.33 mM $Ca(NO_3)_2$, 0.41 mM $CaCl_2$, 2.4 mM $NaHCO_3$, 10 mM HEPES [pH 7.4], 200 mOsmol). Osmotic water permeability (P_f) was determined by measuring the rate of oocyte swelling induced by a hypo-osmotic shock of 180 mOsm/kg. Changes in cell volume were monitored at 15 s intervals. Oocyte volumes (V) at each time point were calculated relative to the initial volume (V_0). The change in the relative volume with time, $d(V/V_0)/dt$, up to 10 min was fitted by a quadratic polynomial, and the initial rate of swelling was calculated. Osmotic water permeability (P_f) was calculated from osmotic swelling data, initial oocyte volume ($V_0 = 9 \times 10^{-4}$ cm^{-3}), initial oocyte surface area ($S = 0.045$ cm^2), and the molar volume of water ($V_w = 18$ cm^3/mol) (Preston et al., 1992):

$$P_f = [V_0 \times d(V/V_0)/dt]/[S \times V_w \times (osm_{in} - osm_{out})]$$

ACCESSION NUMBERS

Nucleotide sequence data from this article can be found in the Arabidopsis Genome Initiative database or GenBank/EMBL databases under the following accession numbers: *Arabidopsis* PIP2;1 (P43286), spinach PIP2;1 (Q41372), and human PIP2;1 (P29972).

SUPPLEMENTAL INFORMATION

Supplemental Information is available at *Molecular Plant Online*.

FUNDING

This work was supported by a grant from the Cooperative Research Program for Agriculture Science & Technology Development (project no. PJ010953012016) Rural Development Administration, Republic of Korea.

ACKNOWLEDGMENTS

We thank Seong Kyu Han for programming to measure van der Waals interaction. No conflict of interest declared.

Received: February 15, 2016
Revised: February 15, 2016
Accepted: April 18, 2016
Published: April 29, 2016

REFERENCES

Becker, D. (1990). Binary vectors which allow the exchange of plant selectable markers and reporter genes. Nucl. Acids Res. **18**:203.

Besserer, A., Burnotte, E., Bienert, G.P., Chevalier, A.S., Errachid, A., Grefen, C., Blatt, M.R., and Chaumont, F. (2012). Selective regulation of maize plasma membrane aquaporin trafficking and activity by the SNARE SYP121. Plant Cell **24**:3463–3481.

Bienert, G.P., Cavez, D., Besserer, A., Berny, M.C., Gilis, D., Rooman, M., and Chaumont, F. (2012). A conserved cysteine residue is involved in disulfide bond formation between plant plasma membrane aquaporin monomers. Biochem. J. **445**:101–111.

Buck, T.M., Wagner, J., Grund, S., and Skach, W.R. (2007). A novel tripartite motif involved in aquaporin topogenesis, monomer folding and tetramerization. Nat. Struct. Mol. Biol. **14**:762–769.

Chevalier, A.S., Bienert, G.P., and Chaumont, F. (2014). A new LxxxA motif in the transmembrane Helix3 of maize aquaporins belonging to the plasma membrane intrinsic protein PIP2 group is required for their trafficking to the plasma membrane. Plant Physiol. **166**:125–138.

de Groot, B.L., and Grubmuller, H. (2001). Water permeation across biological membranes: mechanism and dynamics of aquaporin-1 and GlpF. Science **294**:2353–2357.

Duchesne, L., Deschamps, S., Pellerin, I., Lagree, V., Froger, A., Thomas, D., Bron, P., Delamarche, C., and Hubert, J.F. (2001). Oligomerization of water and solute channels of the major intrinsic protein (MIP) family. Kidney Int. **60**:422–426.

Duchesne, L., Pellerin, I., Delamarche, C., Deschamps, S., Lagree, V., Froger, A., Bonnec, G., Thomas, D., and Hubert, J.F. (2002). Role of C-terminal domain and transmembrane helices 5 and 6 in function and quaternary structure of major intrinsic proteins: analysis of aquaporin/glycerol facilitator chimeric proteins. J. Biol. Chem. **277**:20598–20604.

Emsley, P., Lohkamp, B., Scott, W.G., and Cowtan, K. (2010). Features and development of Coot. Acta Crystallogr. D Biol. Crystallogr. **66**:486–501.

Fetter, K., Van Wilder, V., Moshelion, M., and Chaumont, F. (2004). Interactions between plasma membrane aquaporins modulate their water channel activity. Plant Cell **16**:215–228.

Fu, D., Libson, A., Miercke, L.J., Weitzman, C., Nollert, P., Krucinski, J., and Stroud, R.M. (2000). Structure of a glycerol-conducting channel and the basis for its selectivity. Science **290**:481–486.

Gomes, D., Agasse, A., Thiebaud, P., Delrot, S., Geros, H., and Chaumont, F. (2009). Aquaporins are multifunctional water and solute transporters highly divergent in living organisms. Biochim. Biophys. Acta **1788**:1213–1228.

Hachez, C., Besserer, A., Chevalier, A.S., and Chaumont, F. (2013). Insights into plant plasma membrane aquaporin trafficking. Trends Plant Sci. **18**:344–352.

Haeger, S., Kuzmin, D., Detro-Dassen, S., Lang, N., Kilb, M., Tsetlin, V., Betz, H., Laube, B., and Schmalzing, G. (2010). An intramembrane aromatic network determines pentameric assembly of Cys-loop receptors. Nat. Struct. Mol. Biol. **17**:90–98.

Hedfalk, K., Törnroth-Horsefield, S., Nyblom, M., Johanson, U., Kjellbom, P., and Neutze, R. (2006). Aquaporin gating. Curr. Opin. Struct. Biol. **16**:447–456.

Hessa, T., Reithinger, J.H., von Heijne, G., and Kim, H. (2009). Analysis of transmembrane helix integration in the endoplasmic reticulum in *S. cerevisiae*. J. Mol. Biol. **386**:1222–1228.

Ishibashi, K., Hara, S., and Kondo, S. (2009). Aquaporin water channels in mammals. Clin. Exp. Nephrol. **13**:107–117.

Jin, J.B., Kim, Y.A., Kim, S.J., Lee, S.H., Kim, D.H., Cheong, G.W., and Hwang, I. (2001). A new dynamin-like protein, ADL6, is involved in trafficking from the trans-Golgi network to the central vacuole in *Arabidopsis*. Plant Cell **13**:1511–1526.

Jozefkowicz, C., Rosi, P., Sigaut, L., Soto, G., Pietrasanta, L.I., Amodeo, G., and Alleva, K. (2013). Loop A is critical for the functional interaction of two *Beta vulgaris* PIP aquaporins. PLoS One **8**:e57993.

Kaldenhoff, R., and Fischer, M. (2006). Aquaporins in plants. Acta Physiol. **187**:169–176.

Kaldenhoff, R., Ribas-Carbo, M., Sans, J.F., Lovisolo, C., Heckwolf, M., and Uehlein, N. (2008). Aquaporins and plant water balance. Plant Cell Environ. **31**:658–666.

Kikuchi, S., Hirohashi, T., and Nakai, M. (2006). Characterization of the preprotein translocon at the outer envelope membrane of chloroplasts by blue native PAGE. Plant Cell Physiol. **47**:363–371.

Kim, D.H., Eu, Y.J., Yoo, C.M., Kim, Y.W., Pih, K.T., Jin, J.B., Kim, S.J., Stenmark, H., and Hwang, I. (2001). Trafficking of phosphatidylinositol 3-phosphate from the trans-Golgi network to the lumen of the central vacuole in plant cells. Plant Cell **13**:287–301.

Kjell, J., Rasmusson, A.G., Larsson, H., and Widell, S. (2004). Protein complexes of the plant plasma membrane resolved by Blue Native PAGE. Physiol. Plant. **121**:546–555.

Lee, Y.J., Kim, D.H., Kim, Y.W., and Hwang, I. (2001). Identification of a signal that distinguishes between the chloroplast outer envelope membrane and the endomembrane system in vivo. Plant Cell **13**:2175–2190.

Lee, H.K., Cho, S.K., Son, O., Xu, Z., Hwang, I., and Kim, W.T. (2009). Drought stress-induced Rma1H1, a RING membrane-anchor E3

ubiquitin ligase homolog, regulates aquaporin levels via ubiquitination in transgenic *Arabidopsis* plants. Plant Cell **21**:622–641.

Luu, D.T., and Maurel, C. (2013). Aquaporin trafficking in plant cells: an emerging membrane-protein model. Traffic **14**:629–635.

Maeshima, M., and Ishikawa, F. (2008). ER membrane aquaporins in plants. Pflugers Arch. **456**:709–716.

Mathai, J.C., and Agre, P. (1999). Hourglass pore-forming domains restrict aquaporin-1 tetramer assembly. Biochemistry **38**:923–928.

Maurel, C. (2007). Plant aquaporins: novel functions and regulation properties. FEBS Lett. **581**:2227–2236.

Maurel, C., Verdoucq, L., Luu, D.T., and Santoni, V. (2008). Plant aquaporins: membrane channels with multiple integrated functions. Annu. Rev. Plant Biol. **59**:595–624.

Mitani, N., Yamaji, N., and Ma, J.F. (2009). Identification of maize silicon influx transporters. Plant Cell Physiol. **50**:5–12.

Murata, K., Mitsuoka, K., Hirai, T., Walz, T., Agre, P., Heymann, J.B., Engel, A., and Fujiyoshi, Y. (2000). Structural determinants of water permeation through aquaporin-1. Nature **407**:599–605.

Neshich, G., Mancini, A.L., Yamagishi, M.E., Kuser, P.R., Fileto, R., Pinto, I.P., Palandrani, J.F., Krauchenco, J.N., Baudet, C., Montagner, A.J., et al. (2005). STING Report: convenient web-based application for graphic and tabular presentations of protein sequence, structure and function descriptors from the STING database. Nucleic Acids Res. **33**:D269–D274.

Nyblom, M., Frick, A., Wang, Y., Ekvall, M., Hallgren, K., Hedfalk, K., Neutze, R., Tajkhorshid, E., and Törnroth-Horsefield, S. (2009). Structural and functional analysis of SoPIP2;1 mutants adds insight into plant aquaporin gating. J. Mol. Biol. **387**:653–668.

Preston, G.M., Carroll, T.P., Guggino, W.B., and Agre, P. (1992). Appearance of water channels in *Xenopus* oocytes expressing red cell CHIP28 protein. Science **256**:385–387.

Rojek, A., Praetorius, J., Frokiaer, J., Nielsen, S., and Fenton, R.A. (2008). A current view of the mammalian aquaglyceroporins. Annu. Rev. Physiol. **70**:301–327.

Savage, D.F., Egea, P.F., Robles-Colmenares, Y., O'Connell, J.D., 3rd, and Stroud, R.M. (2003). Architecture and selectivity in aquaporins: 2.5 a X-ray structure of aquaporin Z. PLoS Biol. **1**:E72.

Sorieul, M., Santoni, V., Maurel, C., and Luu, D.T. (2011). Mechanisms and effects of retention of over-expressed aquaporin AtPIP2;1 in the endoplasmic reticulum. Traffic **12**:473–482.

Sui, H., Han, B.G., Lee, J.K., Walian, P., and Jap, B.K. (2001). Structural basis of water-specific transport through the AQP1 water channel. Nature **414**:872–878.

Törnroth-Horsefield, S., Wang, Y., Hedfalk, K., Johanson, U., Karlsson, M., Tajkhorshid, E., Neutze, R., and Kjellbom, P. (2006). Structural mechanism of plant aquaporin gating. Nature **439**:688–694.

Tajkhorshid, E., Nollert, P., Jensen, M.O., Miercke, L.J., O'Connell, J., Stroud, R.M., and Schulten, K. (2002). Control of the selectivity of the aquaporin water channel family by global orientational tuning. Science **296**:525–530.

Takano, J., Wada, M., Ludewig, U., Schaaf, G., Von Wirén, N., and Fujiwara, T. (2006). The *Arabidopsis* major intrinsic protein NIP5; 1 is essential for efficient boron uptake and plant development under boron limitation. Plant Cell **18**:1498–1509.

Tanaka, M., Wallace, I.S., Takano, J., Roberts, D.M., and Fujiwara, T. (2008). NIP6; 1 is a boric acid channel for preferential transport of boron to growing shoot tissues in *Arabidopsis*. Plant Cell **20**:2860–2875.

Theobald, D.L., and Miller, C. (2010). Membrane transport proteins: surprises in structural sameness. Nat. Struct. Mol. Biol. **17**:2–3.

Waight, A.B., Love, J., and Wang, D.N. (2010). Structure and mechanism of a pentameric formate channel. Nat. Struct. Mol. Biol. **17**:31–37.

Wang, Y., Huang, Y., Wang, J., Cheng, C., Huang, W., Lu, P., Xu, Y.N., Wang, P., Yan, N., and Shi, Y. (2009). Structure of the formate transporter FocA reveals a pentameric aquaporin-like channel. Nature **462**:467–472.

Wistow, G.J., Pisano, M.M., and Chepelinsky, A.B. (1991). Tandem sequence repeats in transmembrane channel proteins. Trends Biochem. Sci. **16**:170–171.

Wittig, I., Braun, H.P., and Schagger, H. (2006). Blue native PAGE. Nat. Protoc. **1**:418–428.

Wroblewski, T., Tomczak, A., and Michelmore, R. (2005). Optimization of Agrobacterium-mediated transient assays of gene expression in lettuce, tomato and Arabidopsis. Plant Biotechnol J. **3**:259–273.

Yang, Y., Li, R., and Qi, M. (2000). *In vivo* analysis of plant promoters and transcription factors by agroinfiltration of tobacco leaves. Plant J. **22**:543–551.

Yu, J., Yool, A.J., Schulten, K., and Tajkhorshid, E. (2006). Mechanism of gating and ion conductivity of a possible tetrameric pore in aquaporin-1. Structure **14**:1411–1423.

Zador, Z., Bloch, O., Yao, X., and Manley, G.T. (2007). Aquaporins: role in cerebral edema and brain water balance. Prog. Brain Res. **161**:185–194.

Zelazny, E., Borst, J.W., Muylaert, M., Batoko, H., Hemminga, M.A., and Chaumont, F. (2007). FRET imaging in living maize cells reveals that plasma membrane aquaporins interact to regulate their subcellular localization. Proc. Natl. Acad. Sci. USA **104**:12359–12364.

Zelazny, E., Miecielica, U., Borst, J.W., Hemminga, M.A., and Chaumont, F. (2009). An N-terminal diacidic motif is required for the trafficking of maize aquaporins ZmPIP2;4 and ZmPIP2;5 to the plasma membrane. Plant J. **57**:346–355.